Appendix 1　Model Construction + RNA-seq Sequencing

Successful Establishment of In Vitro CAF Models and Senescence CAF Models

Human embryonic lung fibroblasts (MRC-5) were in vitro induced into CAFs using TGF-β1, and CAF senescence was successfully induced using 5-FU and hydrogen peroxide.

CAF Models: After conventionally culturing MRC-5 cells for 48 hours, the control group was incubated in complete medium for 24 hours. the intervention group was incubated in complete medium supplemented with 10 ng/mL TGF-β1 for 24 hours, and the inhibitor group was incubated in complete medium supplemented with 10 ng/mL TGF-β1 and the TGF-β/SMAD pathway inhibitor SB525334 for 24 hours. Results: MRC-5 cells treated with 10ng/mL TGF-β1 for 24 hours showed significantly increased FAP and α-SMA signaling (red fluorescence). However, when the TGF-β/SMAD pathway inhibitor SB525334 was added, TGF-β1 failed to activate FAP and α-SMA expression. This demonstrates that TGF-β induction triggers expression of CAF-specific markers (FAP and α-SMA) in MRC-5 cells, consistent with CAF characteristics, confirming successful CAF establishment. The TGF-β/SMAD pathway is thus identified as a key pathway in CAF formation. (Figure 1)

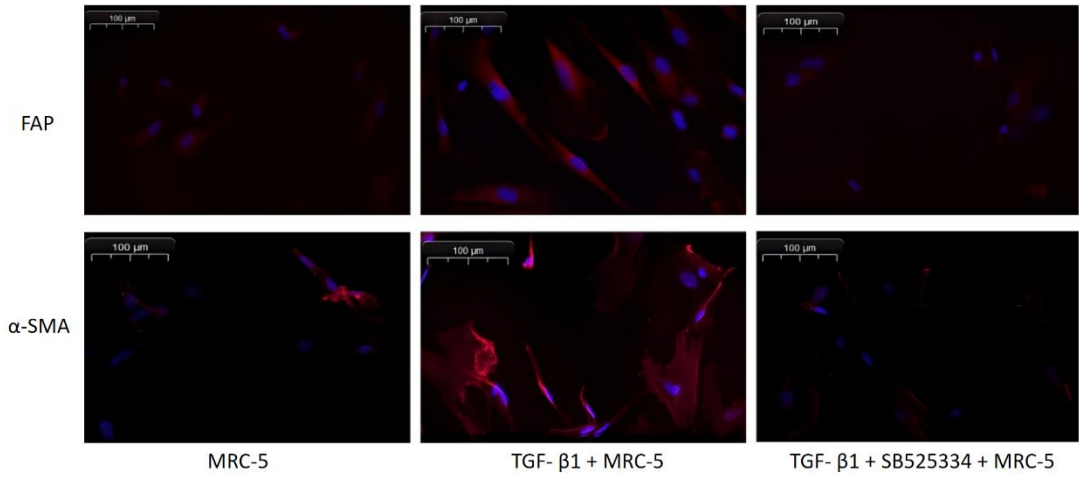

Figure 1 Expression of FAP and α-SMA in Each Group

Senescent CAFs (senCAFs) model: Following the CAF model construction described above, the hydrogen peroxide group was treated with complete medium containing 0.8 mM 5-FU and 60 μM hydrogen peroxide (H_2O_2) for 24 hours, while the 5-FU group was treated for 48 hours. Subsequently, β-galactosidase senescence staining was performed. Results: Both the 5-FU and H_2O_2 groups induced senescence in CAFs (senescent cells stained blue-green), whereas the logarithmic growth phase control group showed negligible senescent cells. Comparing staining ratios between 5-FU and H_2O_2 groups revealed a higher proportion of

senescent cells in the H_2O_2 group, while the 5-FU group exhibited fewer senescent cells but higher cell mortality. (Figure
2)

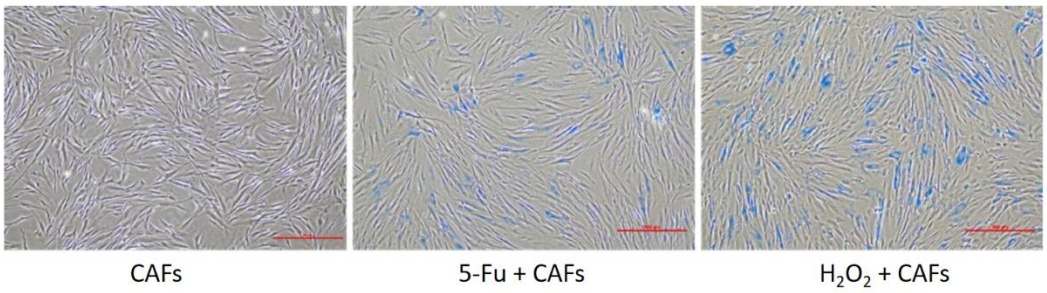

Figure 2 Expression of senescent cells following 5-FU and H_2O_2 treatment

RNA-seq sequencing of senCAFs supports high expression of hyaluronidase (HAase) during SASP.

The DNBSEQ platform was used for RNA-seq sequencing to detect mRNA differences between the normal CAFs group (n=3) and the induced senCAFs group (n=3). A total of 6 samples were measured, yielding an average data size of 1.16G per sample. The average coverage rates for the sample genomes and gene sets were 96.74% and 87.43%, respectively. A total of 17,272 genes were detected, and 9,921 significantly differentially expressed genes were identified through “Reads” filtering (as shown in Figures 3A and 3B).

Among the differentially expressed genes, we screened for SASP components related to matrix remodeling (Figure 3C). This analysis confirmed that the HAase-encoding gene HYAL1 was highly upregulated in the senCAFs group, showing significant differences compared to the control group (Figure 3D). This demonstrates that HA interference may be one of the core functions of matrix-related SASP released by
senCAFs.

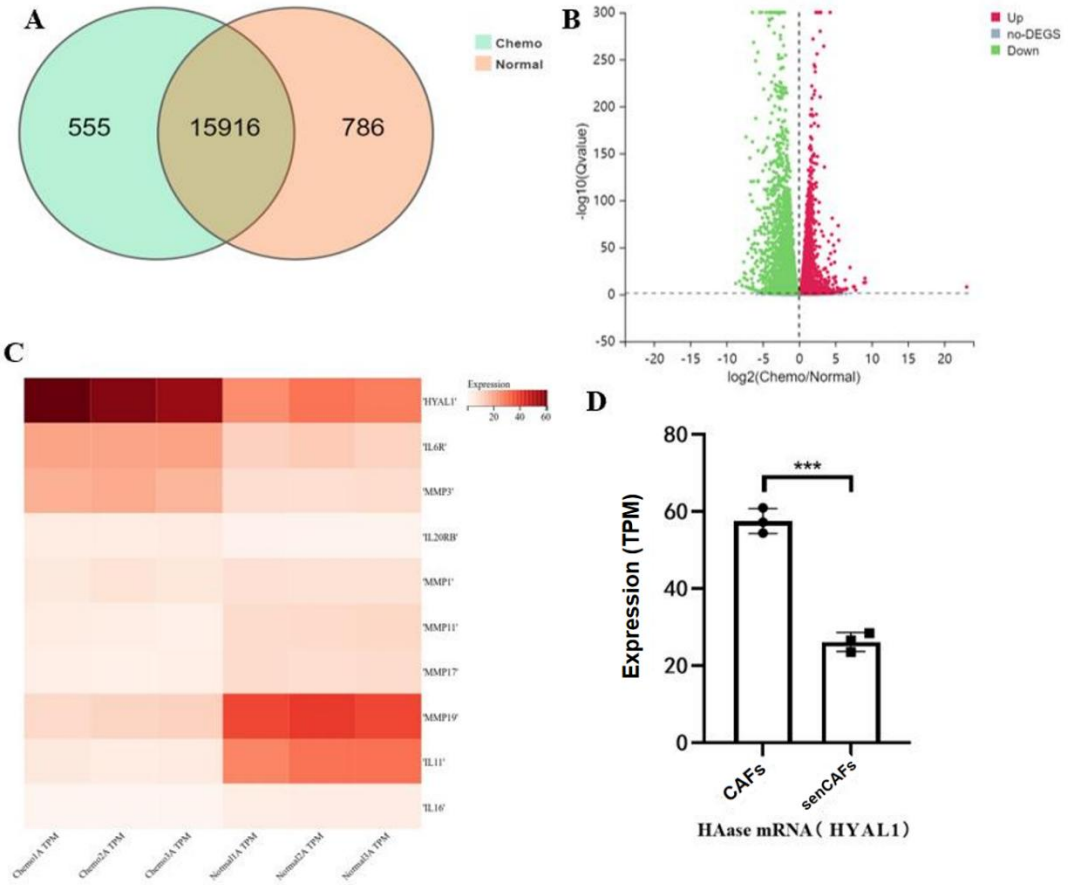

Figure 3 RNA-seq screening of differentially expressed genes in senescent CAFs

Appendix 2　Mass Spectrometry + Pathway Enrichment

***Yiqi Wenyang Jiedu* Prescription (YWJP)**

Astragalus membranaceus 30g, Codonopsis pilosula 15g, Angelica dahurica 10g, Curcuma zedoaria 9g, Paris polyphylla 9g, Polygonum cuspidatum 10g, Smilax glabra root 15g, Atractylodes lancea 10g, total 108g.

Method

Identification of active components in traditional Chinese medicine using an LC-MS system comprising an ACQUITY UPLC I-Class HF ultra-high performance liquid chromatography and a tandem quadrupole high-resolution mass spectrometer. Chromatographic Conditions: Column: ACQUITY UPLC HSS T3 (100 mm × 2.1 mm, 1.8 μm) Column Temperature: 45° C Mobile Phase: A (water containing 0.1% formic acid) and B (acetonitrile) Flow Rate: 0.35 mL/min Injection Volume: 5 μL PDA Scan Range: 210–400 nm

MS Conditions: Ion source: HESI. Acquired in mixed ion mode (MI) for both positive and negative ions. Data acquisition mode: DDA. Scan modes: Full MS/dd-MS2 (TOP 8).

Data Analysis:

Prior to pattern recognition, raw data underwent preprocessing using the metabolomics software Progenesis QI v3.0 for baseline filtering, peak identification, scoring, retention time calibration, and normalization. Compounds were identified based on exact mass, secondary fragments, and isotope distribution. Qualitative analysis was performed using the TCM database to identify the active components of the Yitiguiyang Jiedu Formula.

For substances identified in the QI database, a minimum score of ≥40 was set. A herbal ingredient database for the Yìqì Wēnyáng Jiědù Fāng was established by consulting CNKI, the ITCM database, and the Chinese Pharmacopoeia. Ultimately, 74 compounds were identified in the Yiquan Yiyang Detoxification Formula: 22 from raw Astragalus membranaceus, 13 from Codonopsis pilosula, 19 from Angelica dahurica, 15 from Polygonum cuspidatum, 12 from Smilax glabra, 7 from Atractylodes lancea, 4 from Curcuma zedoaria, and 3 from Paris polyphylla. See Figures 1 and 2, with specific active components listed in Table 1.

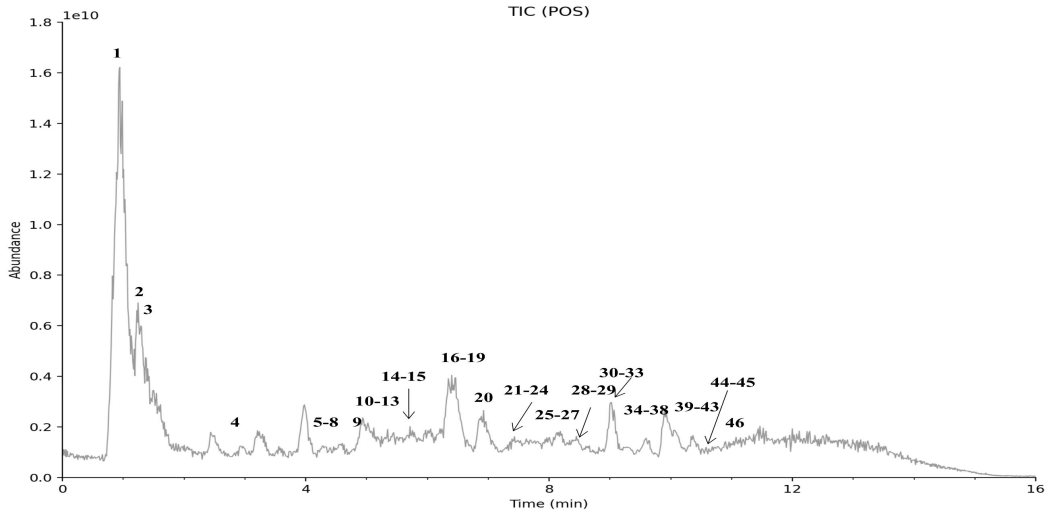

Figure 1 Total Ion Chromatogram (TIC) of the Yiquan Yangde Detoxification Formula: Positive Ion Mode

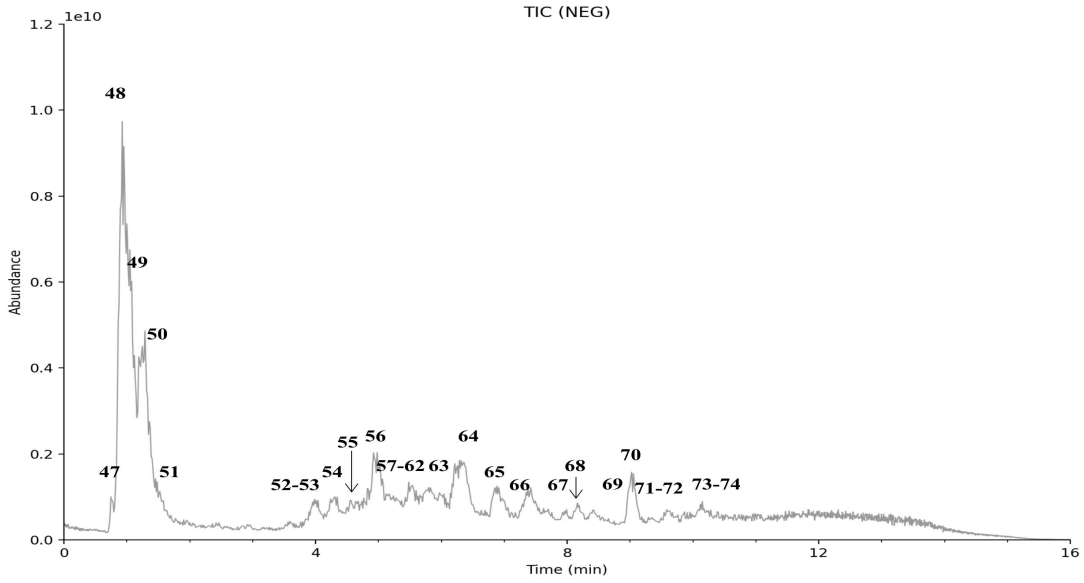

Figure 2 Total Ion Current (TIC) Diagram of the Yiquan Yang-Enhancing Detoxification Formula: Negative Ion Pattern

Table 1 Component Identification Data Matrix for the YWJP

No.	Name	**Chemical formula**	**Retention time /s**	**m/z**
1	Canavanine sulfate	C5H12N403	0.83	177.0982
2	Nicotinic acid riboside	C11H13NO6	1.23	256.0815

3	Arbutin	C12H1607	1.5	290.1238
4	3,5-Dihydroxybenzoic acid	C7H6O4	2.9	155.0338
5	Scopolin	C16H1809	4.25	393.0583
6	Isovanillic acid	C8H8O4	4.39	169.0496
7	Fraxetin	C10H8O5	4.41	209.0446
8	Luteolinidin	$C_{15}H_{11}O_5^+$	4.55	271.0602
9	Resveratroloside	$C_{20}H_{22}O_8$	4.7	391.1384
10	Catechin gallate	$C_{22}H_{18}O_{10}$	5.04	443.0971
11	4,10-Epizedoarondiol	$C_{15}H_{24}O_3$	5.06	275.1609
12	Nodakenin	$C_{20}H_{24}O_9$	5.08	409.1492
13	Isovanillin	$C_8H_8O_3$	5.1	153.0546
14	Lariciresinol	$C_{20}H_{24}O_6$	5.64	361.1639
15	Ononin	$C_{22}H_{22}O_9$	5.69	431.1335
16	Calycosin	$C_{16}H_{12}O_5$	6.35	285.0755
17	Bergaptol	$C_{11}H_6O_4$	6.35	203.0337
18	8-Hydroxybergapten	$C_{12}H_8O_5$	6.48	233.0444
19	Byakangelicin	$C_{17}H_{18}O_7$	6.48	317.1017
20	Kaempferol	$C_{15}H_{10}O_6$	6.76	287.0549
21	Paeoniflorigenone	$C_{17}H_{18}O_6$	7	301.1069
22	Angelicin	$C_{11}H_6O_3$	7.23	187.039
23	Paeonol	$C_9H_{10}O_3$	7.44	149.0597
24	Methoxsalen	$C_{12}H_8O_4$	7.5	217.0496
25	Astragaloside IV	$C_{41}H_{68}O_{14}$	7.82	802.4947
26	Bergapten	$C_{12}H_8O_4$	8.09	217.0496
27	Isopimpinellin	$C_{13}H_{10}O_5$	8.12	247.0601
28	Isomucronulatol	$C_{17}H_{18}O_5$	8.33	303.1225

29	Astragaloside II	$C_{43}H_{70}O_{15}$	8.41	827.4784
30	Arnicolide C	$C_{19}H_{26}O_5$	8.85	335.1849
31	Paris saponin VII	$C_{51}H_{82}O_{21}$	8.86	1048.5688
32	Byakangelicol	$C_{17}H_{16}O_6$	8.98	317.1018
33	Oxypeucedanin	$C_{16}H_{14}O_5$	9.08	287.0913
34	Isoastragaloside II	$C_{43}H_{70}O_{15}$	9.24	849.4603
35	Alloimperatorin	$C_{16}H_{14}O_4$	9.54	271.0964
36	Curcumenol	$C_{15}H_{22}O_2$	9.61	217.1587
37	Atractylenolide III	$C_{15}H_{20}O_3$	9.61	231.138
38	Astragaloside I	$C_{45}H_{72}O_{16}$	9.65	869.4892
39	Isoastragaloside I	$C_{45}H_{72}O_{16}$	9.88	869.4891
40	Zederone	$C_{15}H_{18}O_3$	9.91	247.1328
41	Formosanin C	$C_{51}H_{82}O_{20}$	10.1	1032.5736
42	Imperatorin	$C_{16}H_{14}O_4$	10.11	271.0964
43	Neocurdione	$C_{15}H_{24}O_2$	10.11	254.2114
44	Phellopterin	$C_{17}H_{16}O_5$	10.37	301.1069
45	Quillaic acid	$C_{30}H_{46}O_5$	10.55	469.3311
46	Suberosin	$C_{15}H_{16}O_3$	10.7	245.1172
47	Isocitric acid	$C_6H_8O_7$	0.7	191.0189
48	Arginin	$C_6H_{14}N_4O_2$	0.84	173.1036
49	Citric acid	$C_6H_8O_7$	1.24	191.019
50	Adenosine	$C_{10}H_{13}N_5O_4$	1.41	312.0948
51	Gallic acid	$C_7H_6O_5$	1.92	169.0135
52	Neochlorogenic acid	$C_{16}H_{18}O_9$	3.86	353.0877
53	Epigallocatechin	$C_{15}H_{14}O_7$	3.92	351.0726
54	Chlorogenic acid	$C_{16}H_{18}O_9$	4.27	353.0877

55	Psoralenoside	$C_{17}H_{18}O_9$	4.53	347.0771
56	Polydatin	$C_{20}H_{22}O_8$	4.96	435.1294
57	Genistin	$C_{21}H_{20}O_{10}$	5.01	431.0981
58	Lobetyolinin	$C_{26}H_{38}O_{13}$	5.08	603.2294
59	Marmesinin	$C_{20}H_{24}O_9$	5.08	453.1399
60	Ferulic acid	$C_{10}H_{10}O_4$	5.19	193.0499
61	Lobetyolin	$C_{20}H_{28}O_8$	5.43	441.1764
62	Azelaic acid	$C_9H_{16}O_4$	5.52	187.0969
63	Isomucronulatol 7-O-glucoside	$C_{23}H_{28}O_{10}$	6.09	463.161
64	Ethyl Caffeic acid	$C_{11}H_{12}O_4$	6.64	207.0657
65	Isoastragaloside IV	$C_{41}H_{68}O_{14}$	6.86	829.4599
66	Astragaloside VI	$C_{47}H_{78}O_{19}$	7.25	991.5133
67	Astragaloside III	$C_{41}H_{68}O_{14}$	7.7	829.4603
68	Soyasaponin Ba	$C_{48}H_{78}O_{19}$	8.25	939.4975
69	Rhamnocitrin	$C_{16}H_{12}O_6$	8.84	299.0559
70	Acacetin	$C_{16}H_{12}O_5$	8.88	283.0611
71	Astragaloside II	$C_{43}H_{70}O_{15}$	9.25	871.4707
72	Polyphyllin VI	$C_{39}H_{62}O_{13}$	9.3	783.4184
73	Emodin	$C_{15}H_{10}O_5$	10.14	269.0455
74	Gracillin	$C_{45}H_{72}O_{17}$	10.26	929.4765

Interaction with gastric cancer yields 62 key target points. After constructing and analyzing the association data, extracellular matrix tissues and ECM proteoglycans rank among the most significantly enriched components. Network pharmacology association analysis: For each drug-target gene pair, pathway and process enrichment analysis was performed using the following ontology sources: KEGG Pathway, GO Biological Process, Reactome Gene Sets, Canonical Pathways, CORUM, WikiPathways, and PANTHER Pathway. All genes in the genome were used as the enrichment background. Items with P-values < 0.01, minimum counts $\geqslant$ 3, and enrichment factors > 1.5 were collected and grouped into clusters based on

member similarity. The top three clusters with the highest association were: MCODE_1: Cell Cycle, MCODE_2: Secondary Metabolic Processes, and MCODE_3: Extracellular Matrix Organization. This indicates that matrix regulation is a key component in the Yiyin Yangxie Du Fang formula's prevention and treatment of gastric cancer targets (Figure 1).

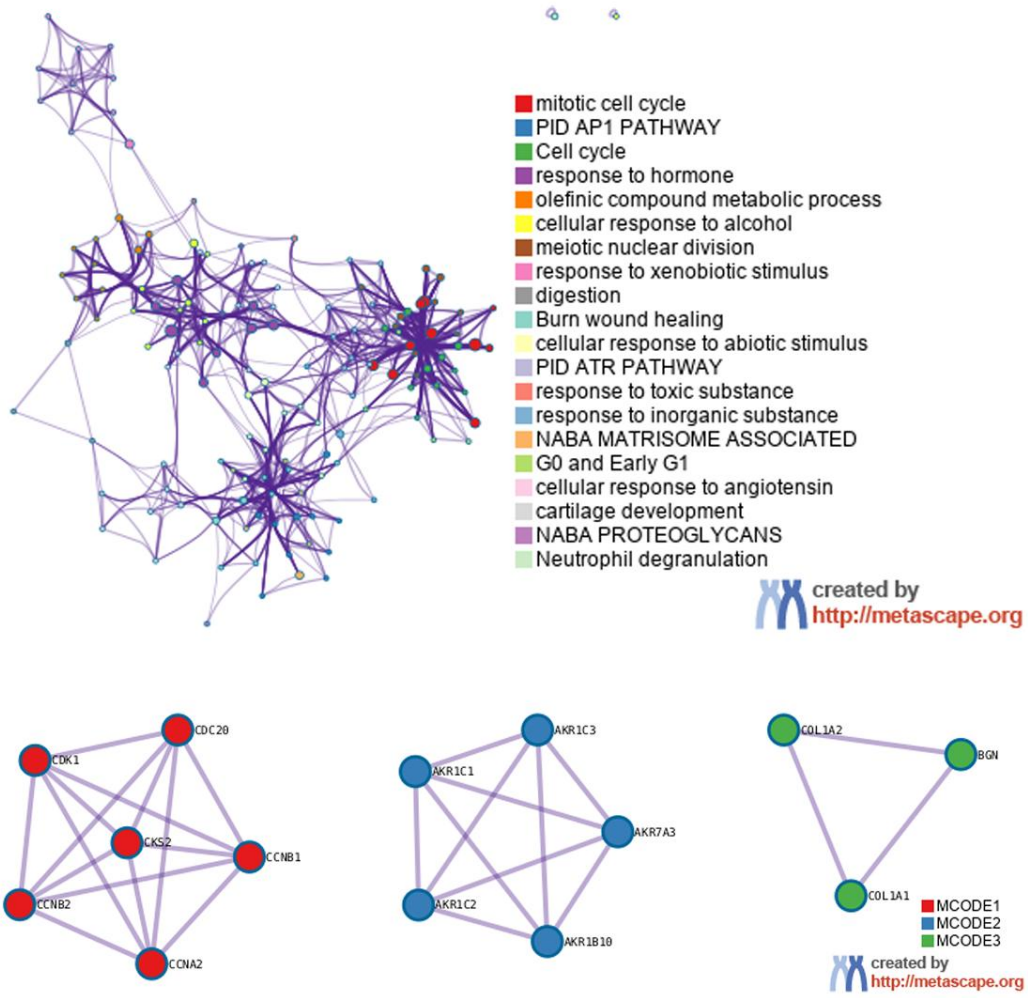

Figure 3 Network Pharmacology Correlation Analysis of YWJP Targets for Gastric Cancer Intervention